Low-Frequency Flexural Wave Acoustic Insulation Characteristics of a Double-Layer Metamaterial Plate

Yu Han, Jingkai Nie, Weimin Xiao, Yi Tian and Qiang He

State Key Laboratory of Advanced Power Transmission Technology (State Grid Smart Grid Research Institute Co., Ltd.), Beijing 102201, China. E-mail: heqiang0927@163.com

Xiaogang Chen

State Grid Zhejiang Electric Power Co., Ltd., Hangzhou 310063, China.

(Received 21 January 2024; accepted 12 April 2024)

The effects of geometric parameters and constituent material parameters on the flexural wave bandgap of a locally resonant double-layer metamaterial plate are investigated using the finite element method. Reasonable parameters are obtained through optimization; then, a double-layer plate made of ABS material with added aluminum mass blocks is designed. The results show that it can open the low-frequency (112–124 Hz) flexural wave bandgap at a subwavelength size. The metamaterial plate is modeled as an equivalent spring-mass system, and the frequency range with negative density for the equivalent dynamic mass is consistent with the width of the flexural wave bandgap. The bandgap generation mechanism is further elucidated. Sound insulation performance of double-layer metamaterial panels verified in an acoustic chamber. The maximum amplitude of STL is achieved at the 112 Hz point in the bandgap frequency range, which indicates that the low-frequency bandgap can effectively reduce vibration and noise. These results demonstrate that this novel double-layer metamaterial plate has wide applications in engineering.

1. INTRODUCTION

With the rapid development of society and the improvement of industrial intelligence, noise from airplanes, high-speed railways, automobiles, and air conditioners has become an extremely severe environmental pollution problem for human beings. Noise affects the normal work, study, and rest of people, causes harm to human health, and possibly damage the human hearing system and affect children's intellectual development.[1] In 2011, the European Commission reported that the social expenditure due to railway and road noise in the European Union was as high as 4 billion euros.[2] The 2021 Annual Report on China Environmental Noise Prevention and Control indicated that in 2020, various levels of environmental protection departments in China organized or undertook a total of approximately 7.45 million yuan in funding for scientific research projects related to the prevention and control of environmental noise pollution. The total output value of the noise and vibration pollution prevention and control industry in China was approximately 12 billion yuan in the same year.[3]

How to control low-frequency noise has always been a hot topic in the field of acoustic. Due to the long wavelength of low-frequency sound waves, the design of noise-reducing materials with a suitable volume for practical applications is difficult. Traditional acoustic methods and technologies cannot effectively control low-frequency noise. Thus, the emergence of acoustic metamaterials has given new life to the ancient field of acoustics in recent years and demonstrates extraordinary physical phenomena that traditional materials do not have, such as negative refraction, acoustic subwavelength imaging, and acoustic perfect absorption.[4–6] Acoustic metamaterials can provide an innovative approach to suppress the propagation of low-frequency sound waves, and many researchers have performed numerous exploratory studies. The Shen research group at the Hong Kong University of Science and Technology bonded an elastic membrane to a relatively rigid plastic grid and attached a circular mass block to each square grid unit cell to form a metamaterial. Experimental results showed a noise reduction performance with a sound transmission loss (STL) of >40 dB in the frequency range of 50–1000 Hz.[7] The Shen research group further designed a metasurface structure with hybrid resonance to absorb subwavelength low-frequency sound, where the structural size was reduced by one order of magnitude.[8] Considering the Helmholtz resonance as an effective method to control low-frequency noise, Zhai et al. in 2019 designed a coupled-resonance acoustic metamaterial using a combination of an open hollow sphere with a negative equivalent elastic modulus and a hollow tube with a negative equivalent mass density.[9] Numerical and experimental results showed perfect low-frequency noise absorption in the frequency range of 750–1000 Hz. The metamaterial size is only approximately 1/8 of the working wavelength, which makes it easy to construct miniaturized noise reduction devices. Subsequently, Li et al. designed a structure that combined microperforated plates and curled cavities.[10] Theoretical calculations and experimental test results showed that the sound absorption coefficient was greater than 0.8 in the frequency range of 262–469 Hz, which indicates that the deep subwavelength structure size has good broadband and high-efficiency sound absorption performance.

Locally resonant metamaterials have become a hot research topic in recent years and can be widely used to control low-

frequency noise and vibration. In 2000, Liu et al. proposed the concept of localized phononic crystals and prepared locally resonant crystals with an equivalent negative elastic modulus in the bandgap near the low frequency of 400 Hz, which reduced the bandgap frequency by two orders of magnitude and was used to control long wavelengths at a small size.[11] To further control low-frequency vibration, Belle et al. arranged S-shaped plexiglass (PMMA) resonant units in a square array on an aluminum plate.[12] They experimentally showed the presence of a low-frequency bandgap at 600 Hz, which was consistent with theoretical calculations. Claeys et al. designed a "sandwich" double-layer honeycomb plate to obtain a bandgap in frequency range of approximately 1000 Hz for flexural waves, and they experimentally validated that this lightweight metamaterial could suppress high-frequency vibrations.[13] Since the local resonance method can be used to design low-frequency metamaterials/structures, De Melo Filho et al. formed a uniform acrylonitrile-butadiene-styrene/polymethyl methacrylate (PMMA) composite material from ABS plastic and PMMA and used thermoforming technology to connect the ABS plastic base plate with the ABS/PMMA structure to form a double-layer plate.[14] Then, they added a 2-mm-thick ABS/PMMA mass block to be periodically distributed on the upper layer of the plate. Theoretical calculations and experimental measurements of STL showed that a narrow flexural wave bandgap could be produced at approximately 150 Hz. Gao et al. Investigated the bandgap property of a thin plate structure with periodically attached double layer membrane-type resonators using plane wave expansion and Rayleigh methods.[15] In addition, Mak et al. proposed the concept of exceeding the causal limit in acoustic absorption and achieved perfect absorption of low-frequency noise at approximately 100 Hz.[16] Xu et al. designed a double-layer perforated plate-type acoustic metamaterial.[17] Ma et al. introduced the structural design methods, acoustic/elastic wave attenuation and regulation principles, and engineering applications of thin-walled acoustic metamaterials for low-frequency sound insulation.[18] Zhou et al. attached multiple layers of rubber and metal cylinders to a thin plate to obtain multiple flexural wave bandgaps in the low frequency range.[19] Langfeldt et al. proposed a plate-type acoustic metamaterial with Helmholtz resonator masses to enhance the sound insulation.[20] Yang et al. proposed a multilayer coupled plate-type metamaterial consisting of a plate-type acoustic metamaterial and a double layer of fibers.[21]

The above studies show that it is challenging to absorb ultra-low-frequency sound in scientific research. Based on the local resonance mechanism,[11] this study designs a double-layer metamaterial plate with periodically distributed U-shaped grooves and microstructural unit cells attached to mass blocks. The new metamaterial plate has a simple structure and is easy to manufacture, so it has great application prospects in reducing vibration and noise for indoor building structures, concert halls, and aircraft cabins. The elastic wave band structure (dispersion curve) of the plate is calculated using the finite element method. Then, the effects of different constituent material parameters, geometric parameters, and mass block thickness values on the flexural wave super bandgap are analyzed. By optimizing these parameters, we construct a new type of double-layer metamaterial plate with a low-frequency bandgap for flexural waves. Furthermore, an equivalent spring-mass system is established to predict the bandgap rationality based on the frequency range with negative density for the dynamic mass. Finally, the sound insulation performance of this double-layer plate metamaterial is verified in the sound insulation room, which can provide technical support for the engineering application of the plate.

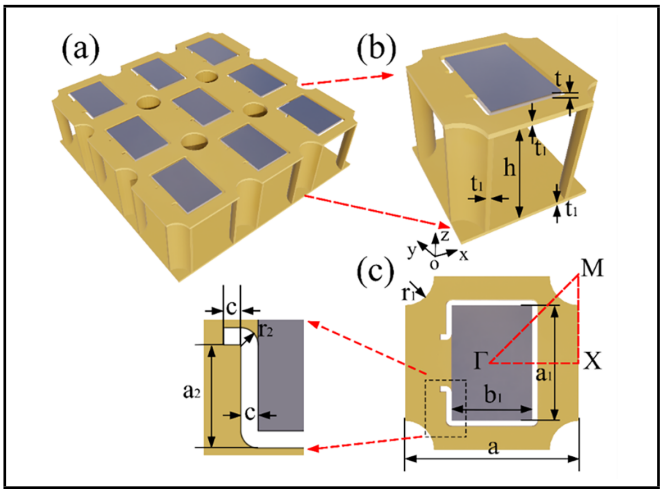

Figure 1. (a) Three-dimensional schematic diagram of metamaterial bipanels with square resonance units, (b) the unit cell, (c) its top view and first Brillouin zones.

2. MODEL BUILDING AND FINITE ELEMENT CALCULATION

Figure 1(a) is a schematic diagram of a three-dimensional (3D) locally resonant double-layer metamaterial plate. The U-shaped grooves in the upper layer of the plate were arranged in a square array, where the grey area represented resonant units; the lower layer of the plate was an isotropic plate; the upper and lower layers were connected by hollow cylinders to create a lightweight, easy-to-manufacture, and structurally simple composite double-layer plate. The unit cells in Fig. 1(b) show the enlarged microstructure of the 3D periodic structure, where the mass block has thickness t and the hollow cylinder has height h. In the top view of Fig. 1(c), the lattice constant was a, and the mass block had length a_1, width b_1, and thickness t; the upper and lower layers of the plate and hollow cylinder had thickness t_1, and the hollow cylinder had an inner diameter of r_1; in the partially enlarged view of the U-shaped groove, the groove had width c, a transition arc radius of r_2, and a groove arm length of a_2; the pink dashed triangle represented the boundary of the first reduced Brillouin zone $\Gamma - X - M$.

When elastic waves propagated in a locally resonant double-layer metamaterial plate, the band structure was calculated using the finite element method. Bloch-Floquet periodic boundary conditions were applied to the unit cell, as shown in Fig. 1(b). After meshing the unit cell using finite elements, the discrete form of the characteristic equation is:[16,22]

$$\left[\mathbf{K}\left(\kappa\right) - \omega^2 \mathbf{M}\right] \mathbf{u} = 0; \tag{1}$$

where κ was the wave vector, ω was the frequency, $\mathbf{u}$ was the displacement vector, $\mathbf{K}$ was the stiffness matrix, and $\mathbf{M}$ was the mass matrix. By scanning the boundary of the first Brillouin zone with wave vector κ, we obtained the elastic

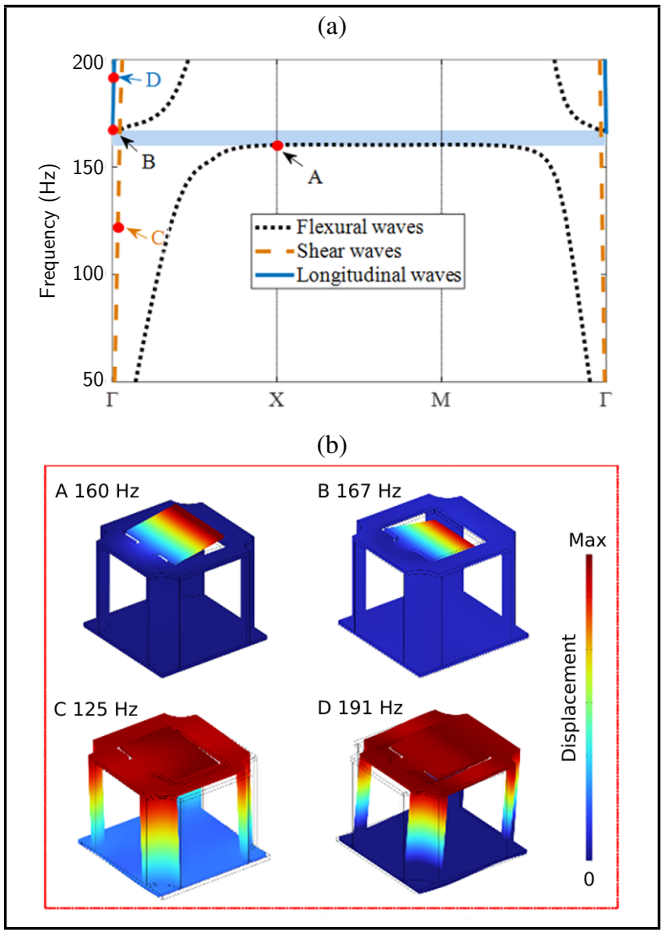

Figure 2. (a) Band structures of metamaterial bipanels for three types elastic waves with the resonance blocks, (b) vibration modes of elastic waves at different frequencies.

wave band structure. Taking the ABS/PMMA composite material as an example, its material parameters were: density $\rho = 971.35$ kg/m^3, Poisson's ratio $\nu = 0.4$, and elastic modulus 1.6×10^3MPa; its geometric parameters were: $t = 0$ mm, $t_1 = 2$ mm, $a = 60$ mm, $h = 46$ m, $a_1 = 36$ mm, $b_1 = 28$ mm, $a_2 = 12$ mm, $r_1 = 10$ mm, $r_2 = 2$ mm, and c =2 mm.

Fig. 2(a) shows the band structures of the longitudinal wave, transverse wave, and flexural wave. In Fig. 2(a), only the flexural wave band has a narrow bandgap of 160–167 Hz. In the vibration mode diagram of elastic waves in Fig. 2(b), points B and A represented the vibration modes of the upper limit (167 Hz) and lower limit (160 Hz) of the flexural wave bandgap, respectively. These vibration modes were mainly manifested by the out-of-plane vibration of the tip of the locally resonant unit of the U-shaped groove in the z-axis direction, whereas the remainder of the unit had relatively insignificant vibration. The vibration mode of the longitudinal wave at Point D (191 Hz) was mainly manifested by resonant units and the upper layer of the plate that vibrates in the *x*-*y* plane. Similarly, the vibration mode of the transverse wave at point C (125 Hz) was manifested by the vibration in the *x*-*y* plane. The vibration modes of these three types of elastic waves show that out-of-plane vibration modes are more likely to produce low-frequency bandgaps.

To obtain a wide low-frequency bandgap, feasible methods were explored by optimizing the design of unit cell geometry parameters and constituent materials.

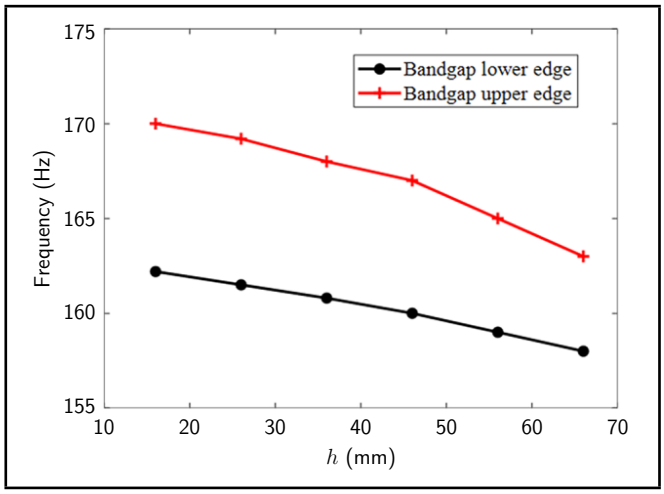

Figure 3. The related curves of flexural wave bandgap and hollow pillar h.

3. DESIGN OF A LOW-FREQUENCY BANDGAP

3.1. Effect of Geometric Parameters on the Bandgap

We selected the material and geometric parameters of the unit cell in Fig. 2 (a) and only considered the change in height h of the hollow cylinder. Fig. 3 shows the finite element calculation results of the low-frequency bandgap for flexural waves. The curve in Fig. 3 shows that when h increased from 16 mm to 66 mm, both upper and lower boundaries of the flexural wave bandgap between the first and second bands tended to be in the low-frequency range, while the bandgap width gradually decreased from a very wide range of 162–170 Hz to a narrow range of 158–163 Hz. Increasing the height h of the hollow cylinder lead to a narrowing of the low frequency band gap. At the same time, the band gap should be in the low-frequency range as much as possible. In addition, the stability of the double-layer plate structure should be considered. Therefore, we selected $h = 46$ mm, which provides a theoretical basis to design a low-frequency locally resonant double-layer metamaterial plate in the next step.

After the height h of the hollow cylinder had been determined to be 46 mm, all geometric parameters in Fig. 1(c) were normalized with respect to parameter h. Figure 4 shows the change curves of the bandgap and lattice constant for the flexural waves, where the dashed line and solid line represented the upper and lower boundaries of the bandgap, respectively. The curve changes show that the bandgap frequency gradually moved toward the low-frequency range when a/h increased. When $0.9 \leq a/h \leq 1$, a very narrow bandgap appears between the first and second bands. When $1.1 \leq a/h \leq 1.3$, a wide bandgap was formed, and a wide bandgap initially opens at $a/h = 1$. When a/h was 1.2 and 1.3, the bandgap widths were 173.5–181 Hz and 160–167 Hz, respectively, which corresponded to lattice constants of 55 mm and 60 mm, respectively. The bandgap curve changes indicated that the lattice constant had a greater influence on the bandgap than the height of the hollow cylinder, or the lattice constant was more sensitive to the bandgap. Because $a/h = 1.3$ can lead to a wide bandgap below 170 Hz and a small lattice constant, it provided a very reasonable size data point to design and prepare ultra-

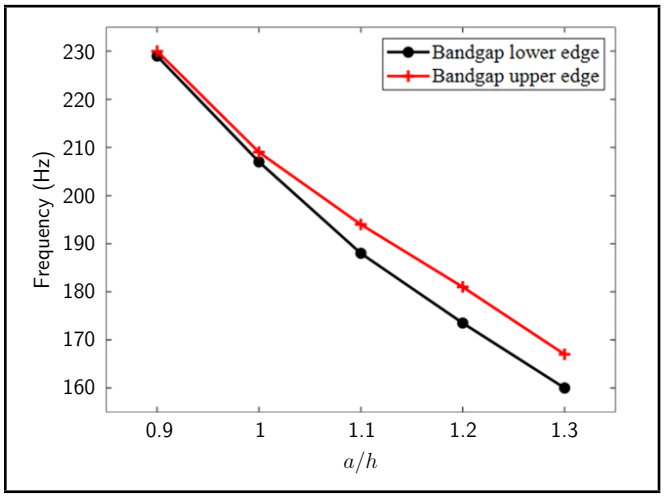

Figure 4. The related curves of flexural wave bandgap and normalized lattice constant a/h.

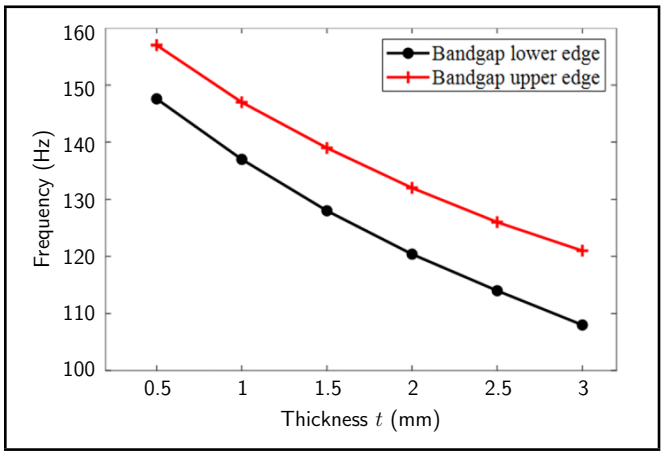

Figure 5. Related curves of flexural wave bandgap and the thicknesses t of different resonance blocks.

low-frequency vibration and noise reduction materials.

In the upper layer of the unit cell plate in Fig. 1(b), we changed the thickness of the mass may help to broaden the low-frequency bandgap. Based on the material and geometric parameters of the unit cell in Fig. 2(a), ABS/PMMA was selected as the material of the mass block. Figure 5 shows the change curves of the upper and lower boundaries of the flexural wave bandgap with thickness t of the mass block. When t increased, the bandgap curve shifts toward the low-frequency range. For example, the bandgap width of $t = 0.5$ mm is approximately 9.4 Hz and the bandgap width of $t = 1.5$ mm was approximately 13 Hz. As the thickness of the mass increases, the band gap of the structure increases slightly. Adding additional mass can shift the band gap of the structure toward lower frequencies.

3.2. Effect of Material Parameters on the Bandgap

In addition to the influence of the key geometric parameters on the bandgap distribution, the constituent materials are an important factor that cannot be ignored. We chose the materials of the additional mass to be iron and aluminum, the thickness of the mass $t = 1$ mm, and the rest of the parameters to be the same as the geometrical parameters of the cell in Fig. 2(a).

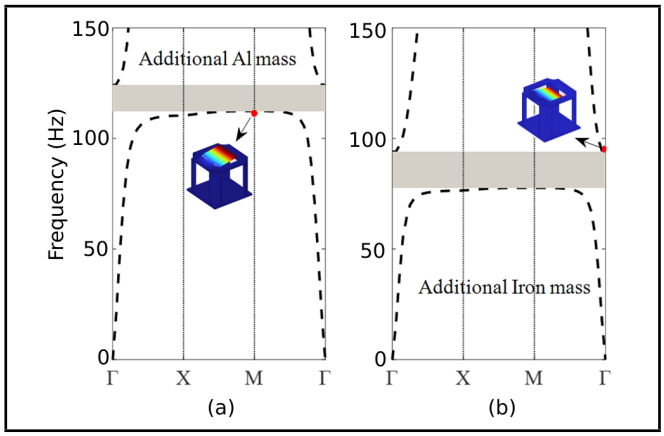

Figure 6. Band structures of flexural waves for metamaterial panels at different resonance blocks.

The material parameters were: density: $\rho_{Iron} = 7850$ kg/m^3 and $\rho_{Al} = 2700$ kg/m^3; Poisson's ratio: $\nu_{Iron} = 0.29$ and $\nu_{Al} = 0.29$; elastic modulus: $E_{Iron} = 2 \times 10^5$ MPa, and $E_{Al} = 7 \times 10^4$ MPa. After adding additional aluminum and iron mass, the theoretically calculated flexural wave band gap of the structure is shown in Fig. 6.

Fig. 6(a) shows that the aluminum mass block produced a flexural wave bandgap of 112–124 Hz. Meanwhile, with an increase in mass density, the iron mass block produced a flexural wave bandgap of 77.6–94 Hz (Fig. 6(b)), which achieved the goal of an ultra-low-frequency broadband bandgap. In Fig. 6(a), the vibration mode at the lower boundary of the bandgap shows that the double-layer plate structure hardly vibrated. The main reason was that the groove-shaped resonant unit and added mass block experience out-of-plane resonance in the z-axis direction, which was like the vibration of a cantilever beam with one fixed end. This phenomenon explains how the local resonance can open the bandgap in the low-frequency region.[16] In comparison, the vibration mode at the upper boundary of the bandgap shows that the added mass block also produced local resonance, and the upper layer of the plate and hollow cylinder have in-plane vibrations in the x-y direction, which were superimposed to form the bandgap in Fig. 6(b).

4. LOCAL RESONANCE MECHANISM AND SOUND INSULATION PERFORMANCE OF THE LOW-FREQUENCY BANDGAP

4.1. Local Resonance Mechanism and Dynamic Mass Density Analysis

For the ABS/PMMA double-layer metamaterial plate and additional aluminum mass block, the low-frequency bandgap results from the local resonance coupling between the U-grooved resonant unit and the double-layer plate structure. When the local energy increased, the flexural wave in the upper layer of the plate and locally resonant unit were coupled to promote the relative motion between different parts of the composite structure and form a low-frequency bandgap.[23] Therefore, the bandgap mechanism can be explained by the dynamic mass density. To calculate the dynamic mass density of the double-layer metamaterial plate, the unit cell in Fig. 1(b) was made equivalent to a two-degree-of-freedom (2DOF) spring-

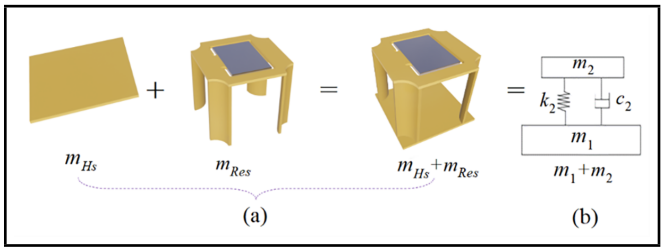

Figure 7. Equivalent dynamic spring mass system of metamaterial unit cell.

mass system as shown in Fig. 7. The dynamic mass equation of the equivalent system was solved, where m_{Hs} and m_{Res} were the masses of the base plate and resonant structure, respectively; m_1, m_2, k_2, and c_2 were the masses, spring stiffness coefficient, and viscous damping coefficient, respectively, of the two vibration units in the equivalent spring-mass system.[23]

For the 2DOF spring-mass system, the dynamic equivalent mass $\widetilde{m}$ is as follows:[23]

$$\widetilde{m}=m_1+m_2\left(\frac{\frac{2j\zeta_2\omega}{\omega_2}+1}{1+\frac{2j\zeta_2\omega}{\omega_2}-\left(\frac{\omega}{\omega_2}\right)^2}\right); \tag{2}$$

where $\zeta_2=\frac{c_2}{2\sqrt{k_2m_2}}$ was the damping ratio of the resonant part, $\omega_2=\sqrt{\frac{k_2}{m_2}}$ was the tunable resonant natural frequency, j was the imaginary unit, and ω was the angular frequency. Solving m_1 and m_2 required the conservation of mass between the unit cell structure and the equivalent 2DOF system, which is expressed as follows:

$$m_1+m_2=m_{Hs}+m_{Res}; \tag{3}$$

Substituting Eq. (3) into Eq. (2) yields the equivalent dynamic mass as follows:

$$\widetilde{m}=m_{Hs}+m_{Res}+\frac{m_{HS}+m_{Res}}{1-\frac{1}{1-(\frac{\omega_H}{\omega_L})^2}}\left(\frac{\frac{2j\omega\zeta_2}{\omega_L}+1}{1+\frac{2j\omega\zeta_2}{\omega_L}-\left(\frac{\omega}{\omega_L}\right)^2}-1\right); \tag{4}$$

where ω_L and ω_H were the lower and upper boundary frequencies of the bandgap, respectively.

When local resonance occurred in the low-frequency range to form a bandgap, only the damping of the resonant structure must be considered. The influence of the base plate on the coupled vibration was negligible. By choosing the parameters $m_{Hs}=0.007$, $m_{Res}=0.0148$, $\omega_L=112$, $\omega_H=124$, and $\zeta_2=2.6\%$, we theoretically calculated the curve of the equivalent dynamic mass density as a function of the frequency according to Eq. (4). The curve in Fig. 8 shows that the equivalent dynamic mass density was negative in the frequency band of 112–124 Hz (shaded area), which was consistent with the bandgap in Fig. 6(a). This result indicates that the locally resonant metamaterial produces a low-frequency bandgap, which results in a negative equivalent dynamic mass, i.e., the structure in this frequency band has a negative response to external excitation. The curve in Fig. 8 shows that there is no resonance at $\omega=0$, so $\widetilde{m}=(m_{Hs}+m_{Res})/a^2$. With the increase in frequency, the equivalent dynamic mass of the system tends to a maximum when the lower boundary frequency of the bandgap is approximately $\omega_L=112$ Hz, sharply drops

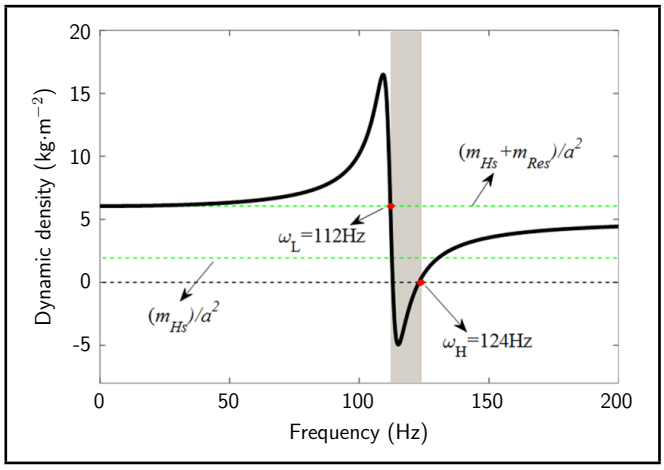

Figure 8. Equivalent dynamic mass density and frequency for metamaterial bipanels.

to a minimum value, and subsequently increases to the upper boundary of the bandgap $\omega_H=124$ Hz ($\widetilde{m}=0$). The negative density obtained by local resonance causes the low-frequency bandgap. When the frequency continues to increase, the resonant structure no longer participates in structural resonance, and the dynamic mass is between the base plate mass $\frac{m_{Hs}}{a^2}$ and static mass $\frac{(m_{Hs}+m_{Res})}{a^2}$ and gradually stabilizes. This process reveals the mechanism by which the local resonance forms the flexural wave bandgap.

To investigate the controlling noise for acoustic waves in this section, the dynamic effective impedance of the metamaterial double panel can be written as:

$$Z_e=i\omega m'; \tag{5}$$

where $m'=\frac{\widetilde{m}}{a^2}$ represented the equivalent mass surface density of the structure. The single-angle incidence sound power transmission coefficient of the metamaterial double panel can be written as:

$$\tau(\theta)=\left|\frac{2}{2+\frac{Z_e\cos(\theta)}{Z_0}}\right|^2; \tag{6}$$

where a transmission factor τ was integrated with the transmission loss. $Z_0=\rho_0c_0$ was the characteristic impedance of air.

To characterize the propagation feature of acoustic waves in the diffuse field, the transmission coefficient $\overline{\tau}$ of the integrated all incidence angles was derived as:

$$\overline{\tau}(\omega)=\frac{\int_0^{\theta_{Max}}\tau(\theta)\cos\theta\sin\theta d\theta}{\int_0^{\theta_{Max}}\cos\theta\sin\theta d\theta}; \tag{7}$$

where θ_{Max} was called the limiting angle above which it was assumed no acoustic waves were received, and varies from 70° to 85°. In the next calculation of $STL=10\log_{10}(1/\overline{\tau})$, θ_{Max} was 85°.

4.2. Experimental Validation

The diffuse transmission loss of the structure was measured in the sound insulation chamber. The sound isolation chamber consisted of two rooms, a sound source room ($4.4\times3\times3$ m) and a semi-anechoic room ($5.2\times3\times3$ m). The two rooms were

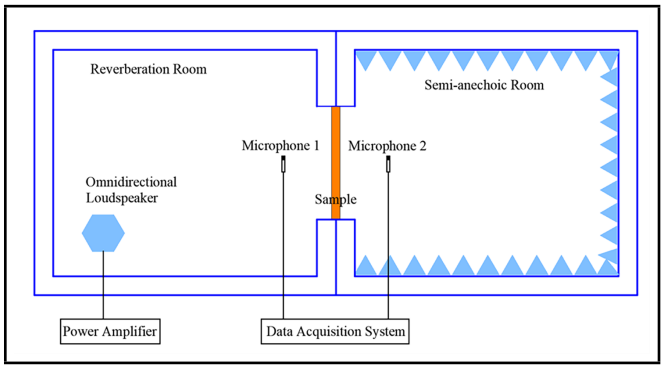

Figure 9. Schematic of the experimental setup used for measurement of diffuse field STL.

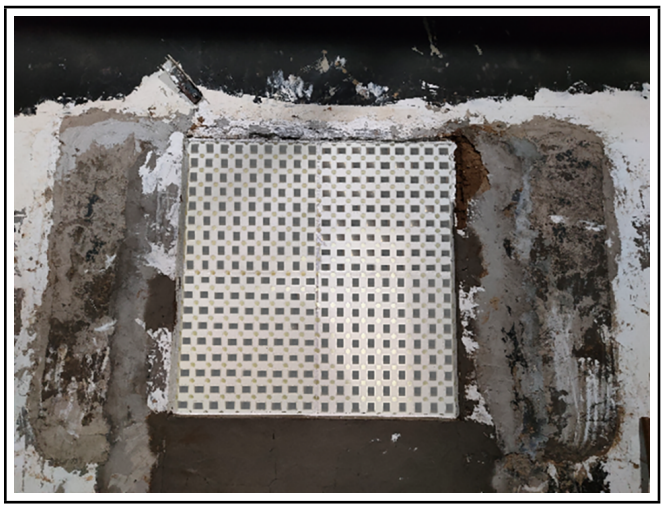

Figure 10. Experimental sample.

connected by a window. The experimental setup for transmission losses is shown schematically in Fig. 9. The sample was mounted on the window as shown in Fig. 10. The frame of the sample is fixed to the edge of the window. The total area of the sample was 980×980 mm. The sample consists of four small pieces. An omnidirectional loudspeaker was placed in the sound source room to create a diffuse sound field in the room. The STL in the experimental test can be obtained by:

$$STL = SPL - SIL + 10lg\frac{S}{A}; \tag{8}$$

where SPL was the average sound pressure level of the reverberation chamber, SIL was the sound intensity level of the semi-anechoic chamber, S is the area of the specimen and A is the absorbing area of the acoustic chamber.

We measured the sound insulation performance of the new structure. The measured diffuse field STLs are presented in Fig. 11. Theoretical calculations of the transmission loss of the diffuse field of the new structure are also shown in Fig. 11. The predicted results are consistent with the trend of the measured transmission losses. The maximum sound insulation of the structure is 23.4 dB at 112 Hz. The minimum sound insulation is 3.4 dB at 126 Hz. The main reason for the higher measured sound insulation is that the four 3D printed cells have additional sides. The overall structure of the structure consists of four cells. This is equivalent to adding reinforcement to the overall structure. On the other hand, the experimental structure is a finite size, whereas the theoretical calculation is an infinite

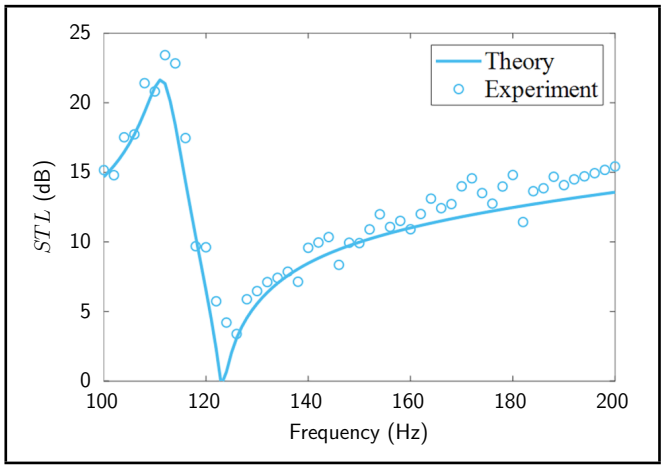

Figure 11. Comparisons of predicted and measured diffuse field STLs.

structure. An increase in the sound insulation of the structure due to the finite size has been reported.[24]

5. CONCLUSION

Based on the local resonance mechanism, this study uses the finite element method to numerically calculate the effects of geometric and constituent material parameters on the low-frequency flexural wave bandgap. On this basis, the design of a locally resonant metamaterial plate with a low-frequency flexural wave bandgap is optimized, the bandgap mechanism is elucidated, and the sound insulation performance is analyzed. By adjusting the thickness of the mass, the band gap of a double-layer plate-type metamaterial can be quickly changed. The double layer metamaterial plate structure is simple in design and easy to manufacture. The main conclusions are as follows:

(1) The optimization results show that the key geometric parameters are: lattice constant $a = 60$ mm, hollow cylinder height $h = 46$ mm, and mass block thickness $t_1 = 2$ mm; the reasonable constituent materials are an ABS/PMMA double-layer plate and an aluminum mass block, which can achieve a desired low-frequency (112–65 Hz) flexural wave bandgap.

(2) Based on the equivalent spring-mass system, the frequency range with negative density that is obtained from the dynamic mass is consistent with the prediction results of the flexural wave bandgap theory, which confirms that the local resonance can open a low-frequency bandgap.

(3) The STL of the structure is measured in an acoustically insulation chamber. The trends of the curves of theoretical predictions and experimental results are in general agreement. The maximum sound insulation of the STL is 23.4 dB at 112 Hz.

In summary, a composite metamaterial plate composed of a non-metallic double-layer plate and a metallic mass block can generate a bandgap in the low-frequency range. The new metamaterial plate has a simple structure and is easy to manufacture. The double layer plate type metamaterial also has good mechanical strength and can be applied in engineering. It has great application prospects in reducing vibration and noise for indoor building structures, concert halls, and aircraft cabins.

ACKNOWLEDGEMENTS

This research was funded by the National Key R&D Program of China (Grant Nos. 2021YFB3801800, 2021YFB3801805).

REFERENCES

[1] Kageyama, T., Adverse effects of community noise as a public health issue, *Sleep Biol Rhythms*, bf14(3), 223-229, (2016). https://doi.org/10.1007/s41105-016-0069-3

[2] Hammer, M. S., Swinburn, T. K., Neitzel, R. L. Environmental noise pollution in the United States: eveloping an effective public health response, *Environ health perspect*, bf122(2), 115-119, (2014). https://doi.org/10.1289/ehp.1307272

[3] Ministry of Ecology and Enviroment of the People's Republic of China: Annual report on China enviroment noise prevention and control, (2021).

[4] Zhang, X. D., Liu, Z. Y. Negative refraction of acoustic waves in two-dimensional phononic crystals, *Appl. Phys. Lett.*, bf93(2), 341-343, (2004). https://doi.org/10.1063/1.1772854

[5] Lu, M. H., Zhang, C., Feng, L., et al. Negative birefraction of acoustic waves in a sonic crystal, *Nat. Mater.*, bf6(10), 744-748, (2007). https://doi.org/10.1038/NMAT1987

[6] Li, Y., Assouar, B. M. Acoustic metasurface-based perfect absorber with deep subwavelength thickness, *Appl. Phys. Lett.*, bf108(6), 063502-1-063502-4, (2016). https://doi.org/10.1063/1.4941338

[7] Yang, Z., Dai, H. M., Chan, N. H., et al. Acoustic metamaterial panels for sound attenuation in the 50-1000 Hz regime, *Appl. Phys. Lett.*, bf96(4), 041906-041906, (2010). https://doi.org/10.1063/1.3299007

[8] Ma, G. C., Yang, M., Xiao, S. W., et al. Acoustic metasurface with hybrid resonances, *Nat. Mater.*, bf13(9), 873-878, (2014). https://doi.org/10.1038/nmat3994

[9] Zhai, S. L., Wang, Y. B., Zhao, X. P. A kind of tunable acoustic metamaterial for low frequency absorption, *Acta Phys. Sin.*, bf68(3), 034301, (2019). https://doi.org/10.7498/aps.68.20181908

[10] Li, D. T., Huang, S. B., Mo, F. S., et al. Low-frequency broadband absorbers based on coupling micro-perforated panel and space-curling chamber, *Chin. Sci. Bull.*, bf65(15), 1420-1427, (2020). https://doi.org/10.1360/tb-2019-0703

[11] Liu, Z. Y., Zhang, X. X., Mao, Y. W., et al. Locally resonant sonic materials, *Science*, bf289(5485), 1734-1736, (2000). https://doi.org/10.1126/science.289.5485.1734

[12] Belle, L. V., Claeys, C., Deckers, E., et al. On the impact of damping on the dispersion curves of a locally resonant metamaterial: Modelling and experimental validation, *J. Sound Vib.*, bf409(24), 1-23, (2017). https://doi.org/10.1016/j.jsv.2017.07.045

[13] Claeys, C., Deckers, E., Pluymers, B., et al. A lightweight vibro-acoustic metamaterial demonstrator: numerical and experimental investigation, *Mech. Syst. Signal Pr.*, bf70-71, 853–880, (2016). https://doi.org/10.1016/j.ymssp.2015.08.029

[14] De Melo Filho N.G.R., Claeys, C., Deckers, E., et al. Realisation of a thermoformed vibro-acoustic metamaterial for increased STL in acoustic resonance driven environments, *Appl. Acoust.*, bf156(15), 78-82, (2019). https://doi.org/10.1016/j.apacoust.2019.07.007

[15] Gao C., Halim D., Yi X. Study of bandgap property of a bilayer membrane-type metamaterial applied on a thin plate, *Int. J. Mech. Sci.*, bf184(1), 105708, (2020). https://doi.org/10.1016/j.ijmecsci.2020.105708

[16] Mak, H. Y., Zhang, X., Dong, Z., et al. Going beyond the causal limit in acoustic absorption, *Phys. Rev. Appl.*, bf16(4), 044062, (2021). https://doi.org/10.1103/PhysRevApplied.16.044062

[17] Xu Y., Wu J. H., Cai Y. Study on dynamic effective parameters of bilayer perforated thin-plate acoustic metamaterials, *Mod. Phys. Lett. B*, 2150048, (2020). https://doi.org/10.1142/S0217984921500482

[18] Ma F., Wang C., Liu C., et al. Structural designs, principles, and applications of thin-walled membrane and plate-type acoustic/elastic metamaterials, *J. Appl. Phys.*, bf129(23): 231103, (2021). https://doi.org/10.1063/5.0042132

[19] Zhou X., Wang L., Qin L., et al. Improving sound insulation in low frequencies by multiple band-gaps in plate-type acoustic metamaterials, *J. Phys. Chem. solids*, bf146(1), 109606, (2020). https://doi.org/10.1016/j.jpcs.2020.109606

[20] Langfeldt F., Khatokar A. J., Gleine W. Plate-type acoustic metamaterials with integrated Helmholtz resonators, *Appl. Acoust.*, bf199, 109019, (2022). https://doi.org/10.1016/j.apacoust.2022.109019

[21] Yang X. H., Kang Y., Xie X., et al. Multilayer coupled plate-type acoustic metamaterials for low-frequency broadband sound insulation, *Appl. Acoust.*, bf209, 109399, (2023). https://doi.org/10.1016/j.apacoust.2023.109399

[22] Osama, R. B., André, F., Chiara, D. Enhancement of deep subwavelength band gaps in flat spiral-based phononic metamaterials using the trampoline phenomena, *J. Appl. Mech.*, bf87(7), 071009, (2020). https://doi.org/10.1115/1.4046893

[23] De Melo Filho, N.G.R., Van Belle, L., Claeys, C., et al. Dynamic mass based sound transmission loss prediction of vibro-acoustic metamaterial double panels applied to the mass-air-mass resonance, *J. Sound Vib.*, bf442, 28-44, (2019). https://doi.org/10.1016/j.jsv.2018.10.047

[24] Villot, M., Guigou, C., Gagliardini, L. Predicting the acoustical radiation of finite size multi-layered structures by applying spatial windowing on infinite structures, *J. Sound Vib.*, bf245(3), 433-455, (2001). https://doi.org/10.1006/jsvi.2001.3592